A Comparative Analysis of CFD ΔP versus Measured ΔP for Maximum Stretched, 4%, 15% and 30% Compressed 6" Diameter Flexible Ducts

ABSTRACT

Computational Fluid Dynamic (CFD) analysis was used to study the pressure drop behavior of six inch (6") diameter flexible duct with a single helix core. The simulation used a positive pressure, blow-through configuration. There are two objectives of this study. First is to set-up a 3-D modeling and mesh generation method of flexible duct, which represents the duct geometry and provides visual information on the flow patterns. Second is to calibrate the CFD model by comparing simulation data with the laboratory data with the same duct configuration. Simulations, based on different duct compressions including fully stretched, 4% compression, 15% compression, and 30% compression, were conducted under a range of air volumes from 70 to 160 cfm in 10 cfm increments. The internal mesh was configured to match the axial length of the spiral. Static pressure data was taken from the CFD analysis for these periodic points. This data from the central axis was then compared to the laboratory data. The results suggested that the CFD model can simulate static pressure drop within about 5 to 10% of the measured values for flexible ducts in the board supported configuration.

INTRODUCTION

As stated in Ugursal et al. (2006), non-metallic flexible ducts are widely used because of low cost and ease of installation. Flexible ducts have limited references since most work has been performed on rigid metal ducts. The ASHRAE Handbook – Fundamentals Chapter 35 provides data on the Pressure Drop Correction Factor for flex for the percent of compression extending to 30% (ASHRAE 2005, Figure 8, page 35.7, data from Abushakra). Abushakra et al. (2004) studied the pressure drop inside fully stretched, 15% compressed and 30% compressed flexible ducts. In current research, Weaver studied the pressure drop in fully-stretched, 4% compressed, 15% compressed, 30% compressed and 45% compressed 6", 8", and 10" diameter flexible ducts (Weaver et al. 2006). In this study, we investigated the mesh configuration for fully stretched, 4% compressed, 15% compressed and 30% compressed flexible ducts. A Computational Fluent Dynamics (CFD) software package (Fluent 2004) generated the flow patterns and pressure drops and was calibrated by comparing the simulation results to experimental measurements by Weaver et al. The results match the laboratory data within about 5% to 10%.

In the first part of this study, we examined the effect of the number of iterations which were used to solve each problem. A comparative graph shows the difference between the different number of iterations. Following this, we studied the pressure loss along a 5' length duct for all four duct configurations under ten volumetric air-flows. In the next section, we presented the extrapolated results of 3', 4', and 5' ducts to a 100' duct. These results are compared to laboratory data for an accuracy check. In the final section, we studied multipliers for 4% and 15% compressions for simulation results agree with the experimental results.

METHODOLOGY

In this study, the three-dimensional (3-D) computer model and the associated mesh were built and executed with commercial CFD software (Fluent 2004, Gambit 2004a). A 6" diameter flexible duct with a 5' length was generated in 3-D with several configurations including maximum stretched, 4% compressed, 15% compressed, and 30% compressed. The actual laboratory experiments were measured on 100' length duct sections. A 5' duct length was used to develop CFD simulations due to the limitations of the software and the computational capabilities of the supercomputer. A two foot (2') straight duct was added to each end of the flexible duct being simulated (Figure 1) to emulate the inlet and outlet boundary conditions used

in acquiring the measured data and to minimize turbulence due to discontinuities at the boundary. The 3-D model in this study corresponds with the board-supported configuration of the laboratory experiment, which lies on a flat surface without any sag.

A semi-empirical standard *k-ε* turbulence model was used in CFD calculations of this study. This model has been used for the turbulence modeling at different scales. Zhang (2005) stated that standard *k-ε* is the most popular of the two-equation models and is able to give satisfactory results for complex flows. Drori et al. (2005) used standard k-*ε* model to simulate airflow inside a 7.7 ft x 7.7 ft x 19.5 ft test room. In a recent study, Koskela (2004) used k- *ε* model to simulate nozzle duct air distribution method. Gan and Riffat (1995) stated that the standard *k-ε* model is suitable to represent turbulence parameters of air in ducts, because air velocity inside the HVAC ducts is high which creates a well-developed turbulent flow. In this study using the standard *k- ε* model, it is assumed that the flow is fully turbulent and the effects of molecular viscosity are negligible (Fluent 2005). 'Velocity inlet' and 'outflow' boundary conditions were used in the simulation. Velocity inlet allows the flow velocity to be defined at the inlet. The outflow boundary condition was used because the pressure for the exiting flow was not specified prior to the solution of the problem.

CFD simulations were conducted for all four duct configurations under ten volumetric air flows, from 70 cfm to 160 cfm. First, static pressure drop in 5', 4' and 3' length duct sections, which are symmetrical to the mid-point, were derived. Since the laboratory setting is a 100' length duct, data from the CFD simulations were multiplied by the factor of 20, 25 and 33.33, respectively. The extrapolated simulation results were then compared to the laboratory data. Second, data from an alternative 3' length section, which was positioned on a length exhibiting a well-developed flow pattern, was extracted and compared to the laboratory data. After the first foot of duct, the data exhibited a well-developed flow since the ΔP per length became constant. Third, 4% and 15% compressed CFD models were tuned by using multipliers until they showed close agreement with the laboratory results. Several possibilities exist for the discrepancy between the CFD models and actual measurements. The CFD assumes that the blow through configuration produces fully-rounded inner core geometry, which may not be the case for smaller compressions. Various configurations are currently under investigation to determine the reasons for these discrepancies.

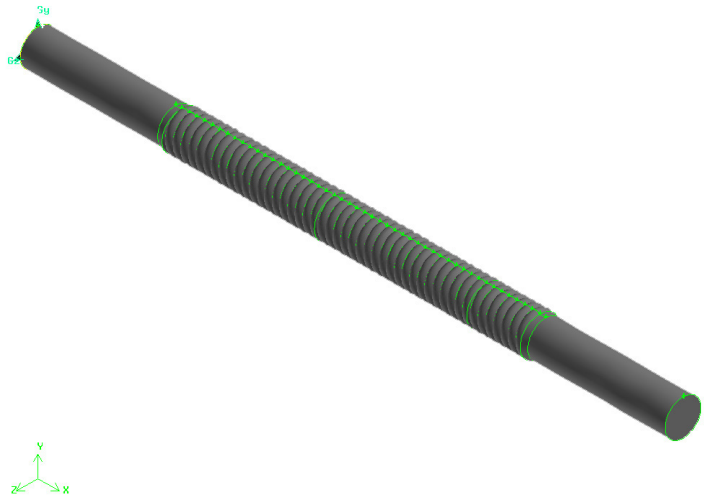

Figure 1. Five-foot long flexible duct with two-foot long additions on both ends.

3-D MODELING OF DUCTS

The basic structure of flexible duct was discussed in Ugursal et al. (2006). A two-ply, polyester inner wall contains a helix shaped steel wire to maintain the dimensional integrity. In the 6" duct being simulated, each 360° turn of the helix core equals a distance of 1.5" along the central axis when fully stretched. The length of the center section for each duct configuration is determined by multiplying the

distance of one segment with an integer to have the closest value to 5 feet. Therefore, the center section of fully-stretched, 4%, 15%, and 30% compressions has a length of 60", 59.925", 59.04" and 59.85", respectively.

The 3-D model of the flexible duct consists of fully inflated curved surfaces with a cusp located along the wire (Figure 2). The central core mesh consists of a standard straight linear grid. The inflated regions required adaptable mesh geometry, adjusted to the inflated inner duct boundary. A structured grid algorithm failed to represent the model. Thus, an unstructured 'pave' face meshing scheme was applied to ensure the geometric representation of the wall surface. The unstructured algorithm provided flexibility for modeling the inflated region of the duct. The volume was then meshed using the 'Hex/Core' scheme which created a core of regular hexahedral elements surrounded by transition layers of tetrahedral, pyramidal, and wedge elements (Gambit 2004b). The final mesh has around 1,300,000 cells which slightly differs for each compression factor.

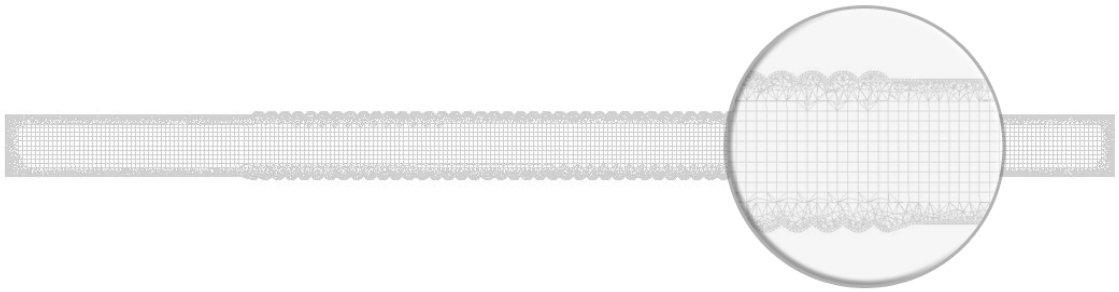

Figure 2. CFD output of duct model and the meshing scheme.

RESULTS

The analysis proceeded in the following sequence. First, the iteration test was run to determine the static pressure drop in a 5' duct section for all four duct configurations. Next, the simulated results from the 5', 4', and 3' long duct sections were extended to have 100' long duct ΔPs, to provide the standard representation of X in-H_20/100' of pressure drop. Finally, the correction factors were derived for 4% and 15% compressions.

Iteration Test

The "Iteration Test," shown in Figure 3, shows how the axial pressure drop changes as a function of the number of numeric iterations in the CFD calculation. The solution becomes more refined as the number of iterations increases. Increasing the iterations results in increased computation time and associated costs, which become limitations as the number of iterations per simulation increases. We applied iteration tests for all four flexible duct configurations to attain the optimum number. The optimal number of iterations for the 4% compressed duct was 130 iterations, as shown in Figure 3. Increasing the iterations beyond 130 did not result in improved performance.

The solution for the flexible duct section, which is between 24" and 89.04", does not differ between 100, 120 and 130 iterations. However, 100 and 120 iterations indicate a backflow in the 2' length end-section which represents an artifact of the CFD calculations. Although 100 iterations would be enough for the purposes of this study, we used 130 iterations to eliminate the "backflow." This optimizes the solution convergence for the 4% compression. Similarly, maximum stretched, 15% compressed, and 30% compressed duct configurations optimally converged at 155, 127, and 164 iterations, respectively. Therefore, these values are used for the simulations. Figure 4a through 4c shows the comparison of three different values of iterations for different airflows, showing that a higher number of iterations produced results with reduced artifacts.

Super computer of the Texas A&M University was used for the computations of this study. The particular machine that we used has 64 processors of 1000 MFLOPS floating speed and has 64 GB of shared memory. We used 16 processors in parallel with up to 2GB memory for each volumetric airflow which took around 20 min. to converge.

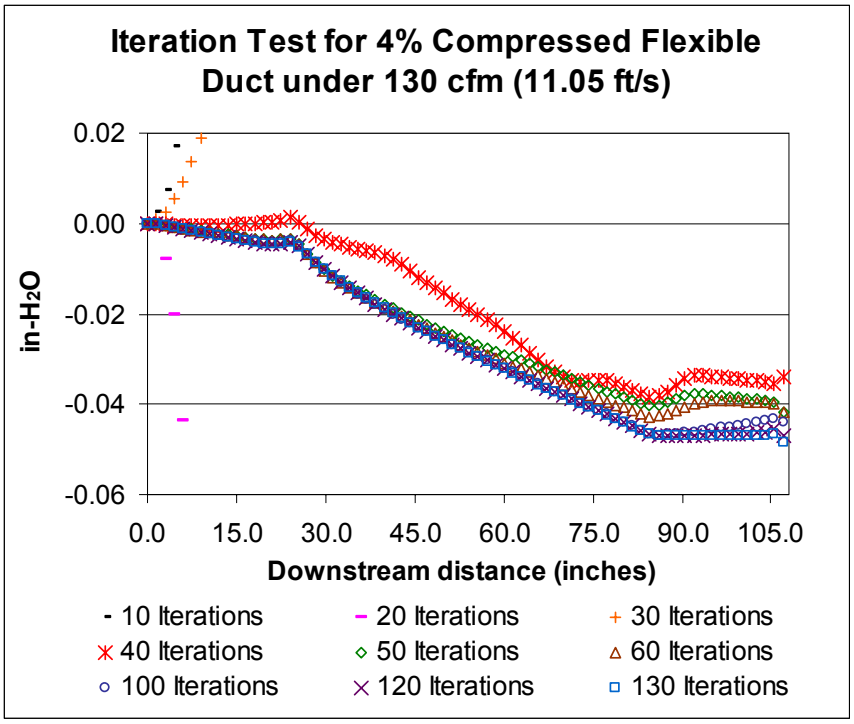

Figure 3. The effect of nine different numbers of iterations on the static pressure simulation.

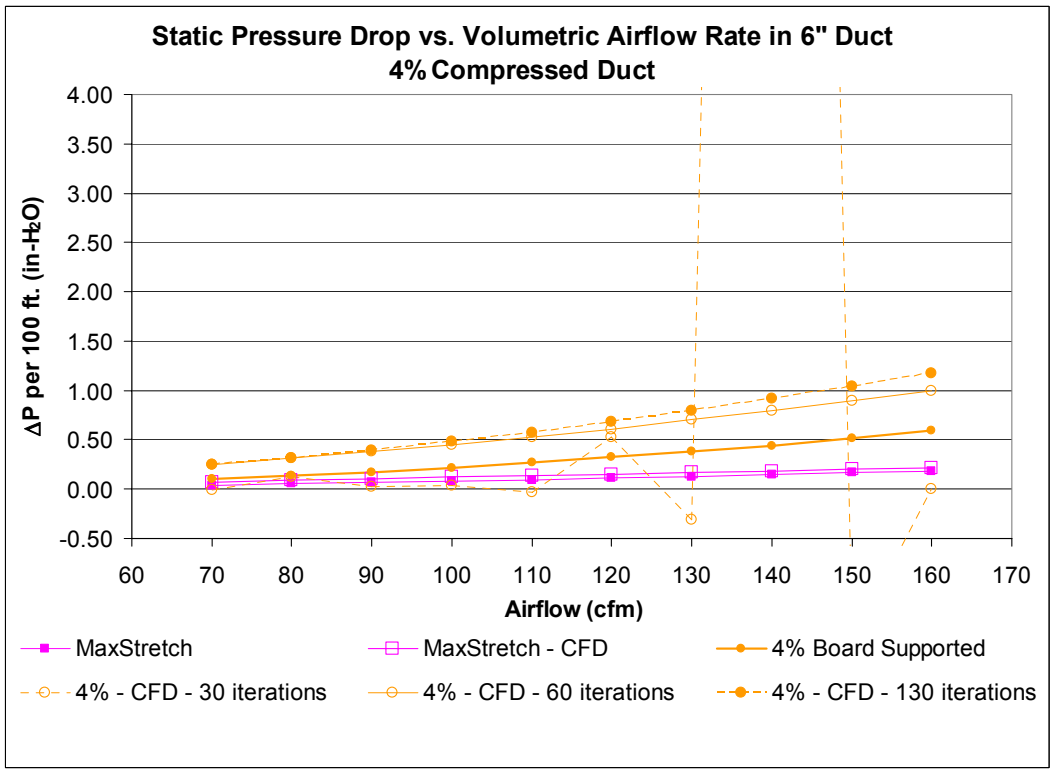

Figure 4a. Comparison between three numbers of iterations for 4% compressed duct.

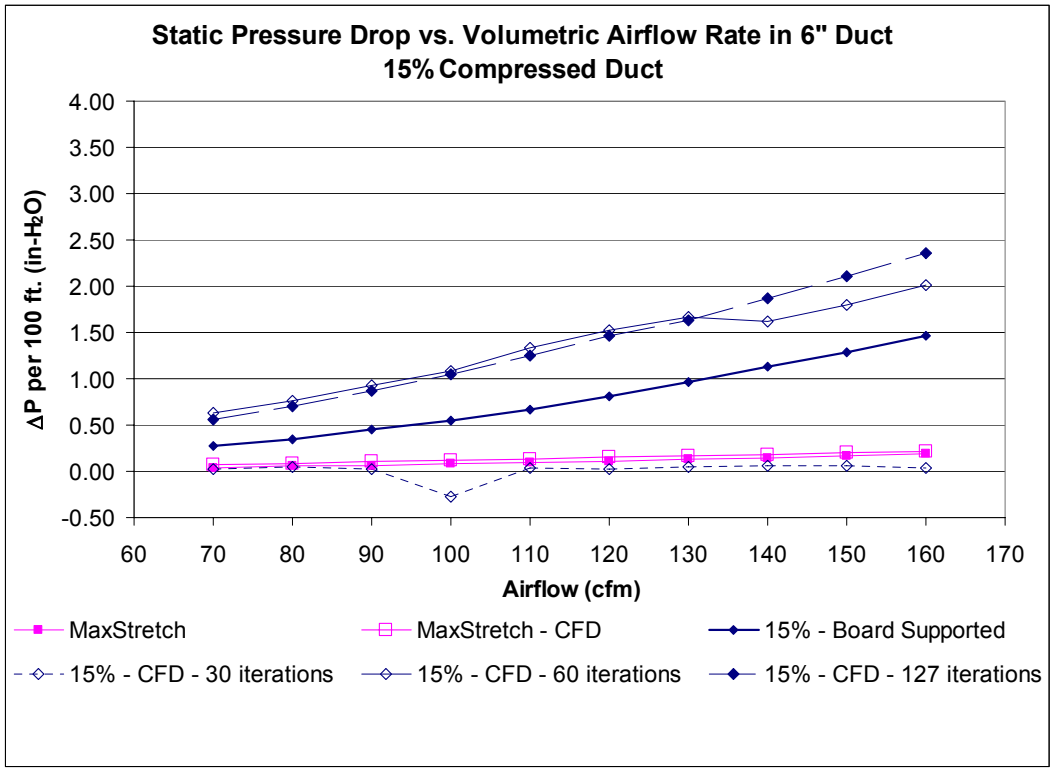

Figure 4b. Comparison between three numbers of iterations for 15% compressed duct.

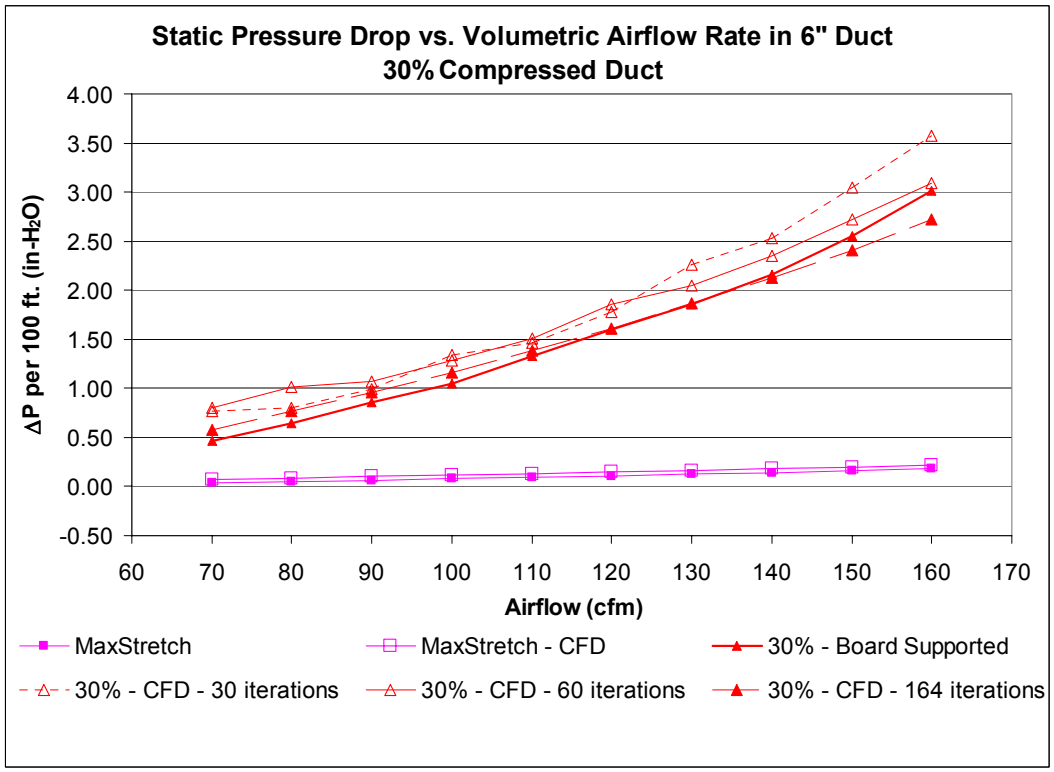

Figure 4c. Comparison between three numbers of iterations for 30% compressed duct.

Static Pressure Drop along the Central Axis

Data points along the central axis were determined based on the travel distance of the helix core at each full turn. Static pressure data was extracted for those data points and presented in Figure 5a through Figure 5d for all configurations. These graphs show the static pressure change along the 5' flexible duct and the two 2' straight end sections. Table 1 presents the simulation results of static pressure difference (ΔP) along the flexible duct portion. These values are then multiplied by 20 to represent the pressure drop as the number of in-H_20/100'. In Figure 6a through Figure 6d, the static pressure difference (ΔP) between each data point is plotted. These graphs indicate that the flow is fully developed after the first one-fifth of the flexible duct section. In a later analysis, the fully developed flow data will be presented in comparison with the laboratory results.

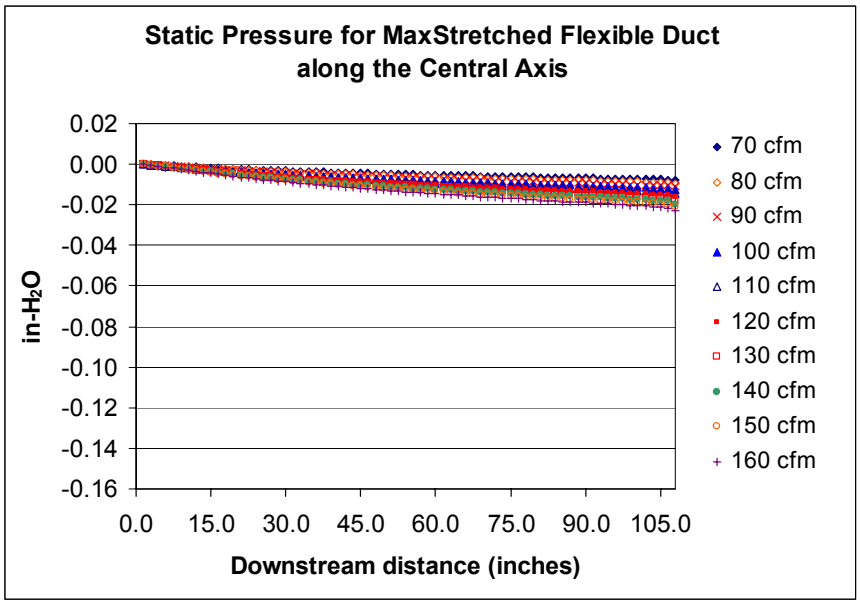

Figure 5a. Static pressure along the fully-stretched flexible duct.

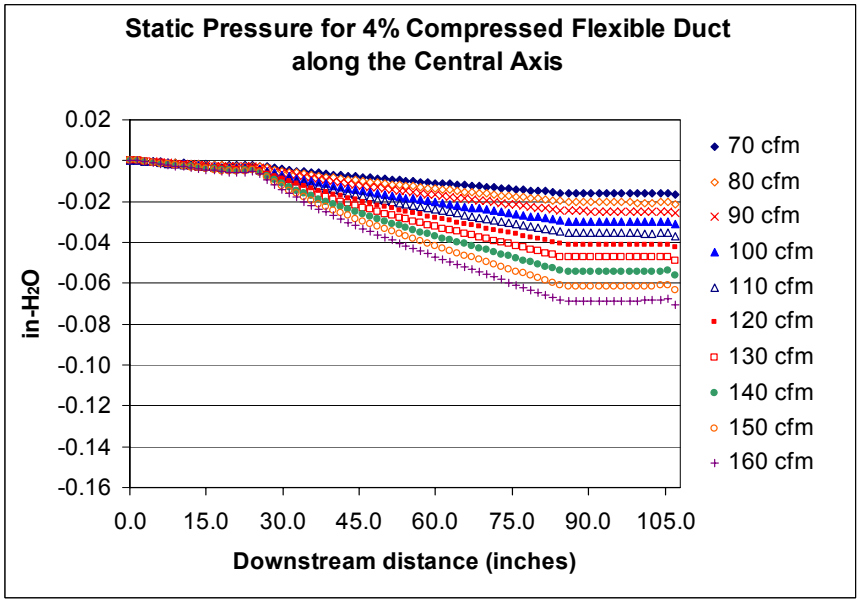

Figure 5b. Static pressure along the 4% compressed flexible duct.

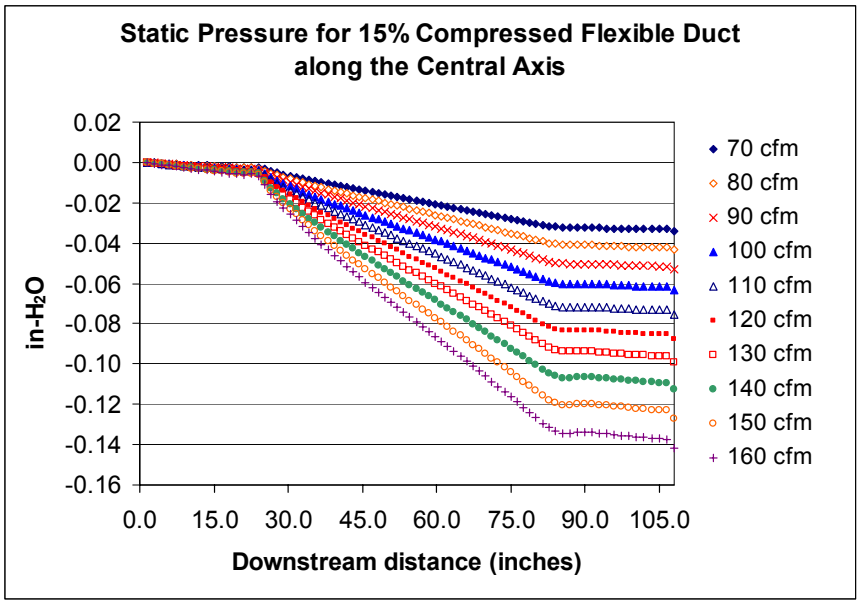

Figure 5c. Static pressure along the 15% compressed flexible duct.

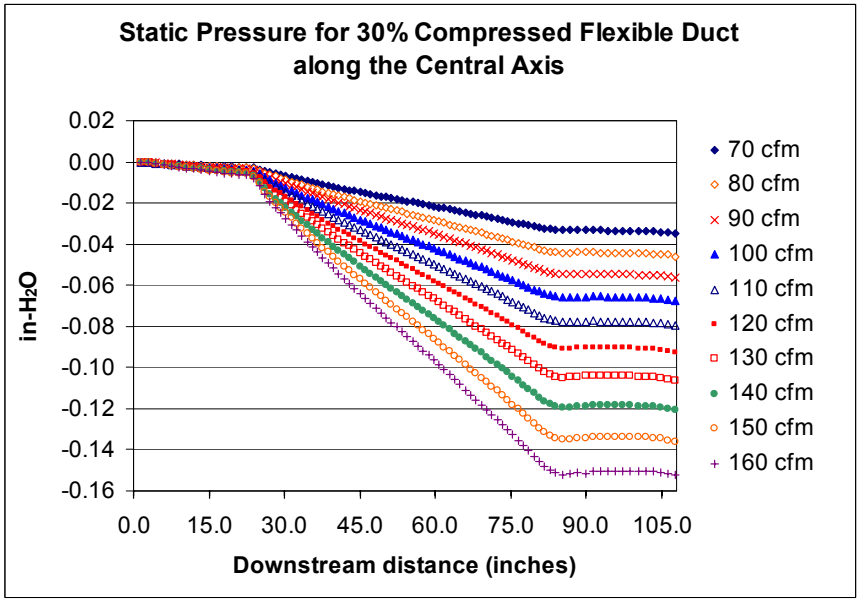

Figure 5d. Static pressure along the 30% compressed flexible duct.

In actual measurements, the duct length needs to be long enough to allow "well developed flow" to occur. In real systems, the airflow inserted into a real duct does not have a uniform cross-sectional velocity. The settling out length typically requires at least 10 duct diameters. Using CFD, a uniform flow can be created at the cross sectional input area. Figures 5b through 5d show the changes settling out to a stable repetitive value in approximately 6 to 8 increments of the spiral coil. Figures 6b through 6d show the change in ΔP from one location to the next location, one spiral coil increment further along the longitudinal axis of the duct. Therefore, we concluded that the length of the simulation domain is adequate for the purpose of this study. Longer domain would not provide more information but require more the computation resources.

TABLE 1
Static Pressure Differences in the 5' Long Flexible Duct Section under Various Volumetric Air-flows

cfm	70	80	90	100	110	120	130	140	150	160
ΔP for MaxStretch in 5 ft.	0.0038	0.0045	0.0053	0.0061	0.0069	0.0078	0.0086	0.0094	0.0102	0.0111
ΔP for 4% in 5 ft.	0.0131	0.0168	0.0209	0.0254	0.0305	0.0359	0.0418	0.0483	0.0550	0.0621
ΔP for 15% in 5 ft.	0.0294	0.0374	0.0463	0.0557	0.0667	0.0781	0.0878	0.1002	0.1131	0.1266
ΔP for 30% in 5 ft.	0.0302	0.0406	0.0504	0.0611	0.0725	0.0849	0.0983	0.1122	0.1272	0.1435

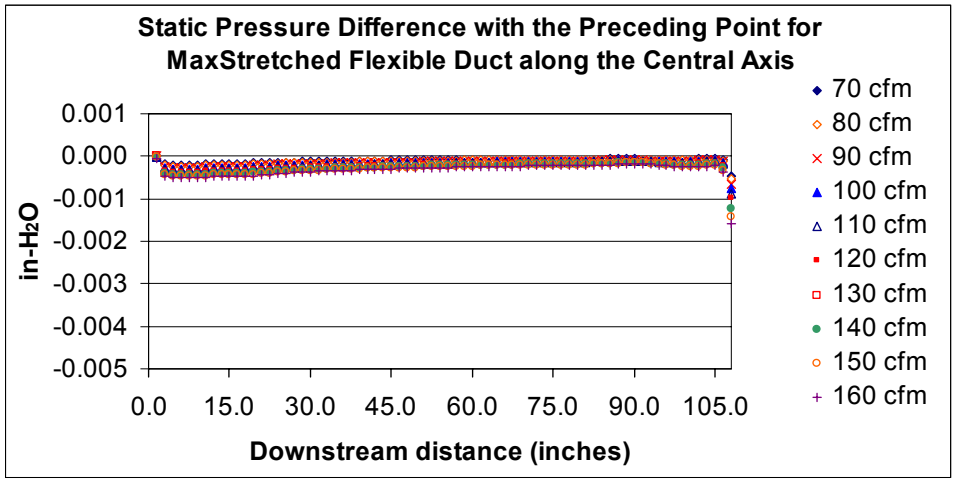

Figure 6a. Static pressure difference with the preceding data point of fully-stretched, flexible duct.

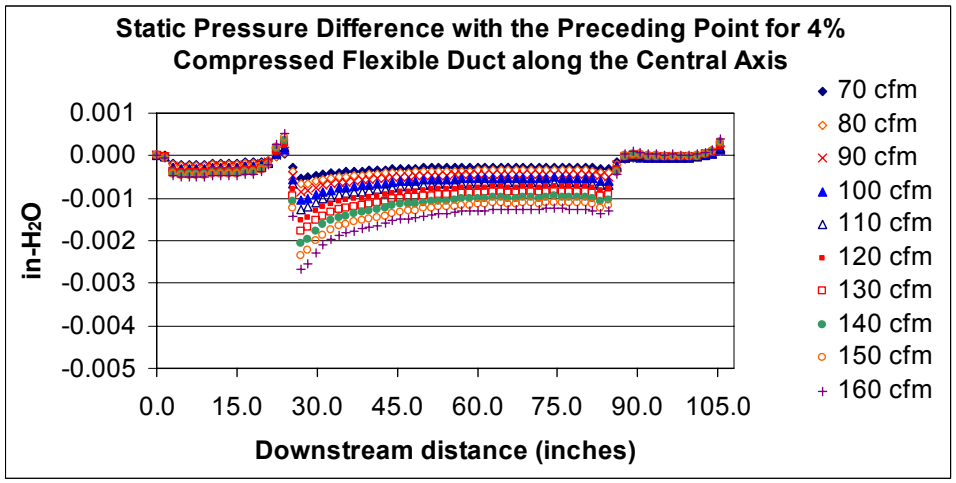

Figure 6b. Static pressure difference with the preceding data point of the 4% compressed flexible duct.

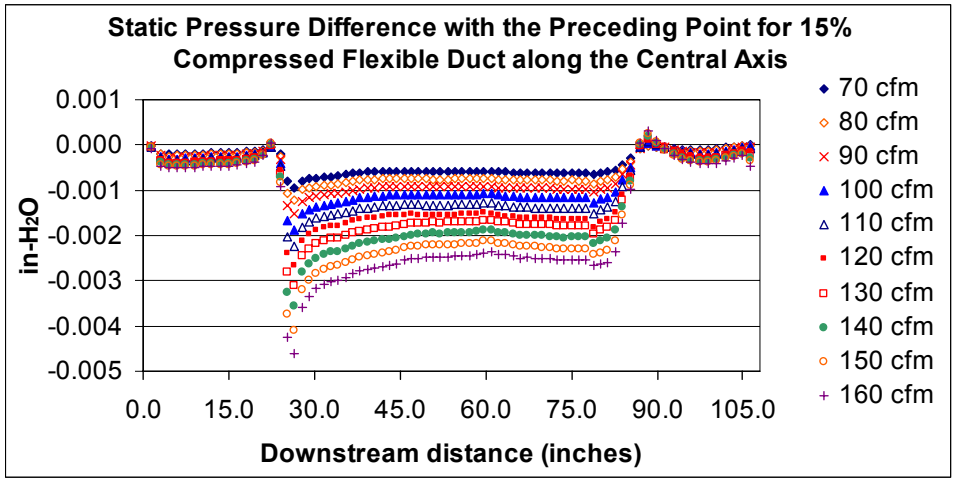

Figure 6c. Static pressure difference with the preceding data point of the 15% compressed flexible duct.

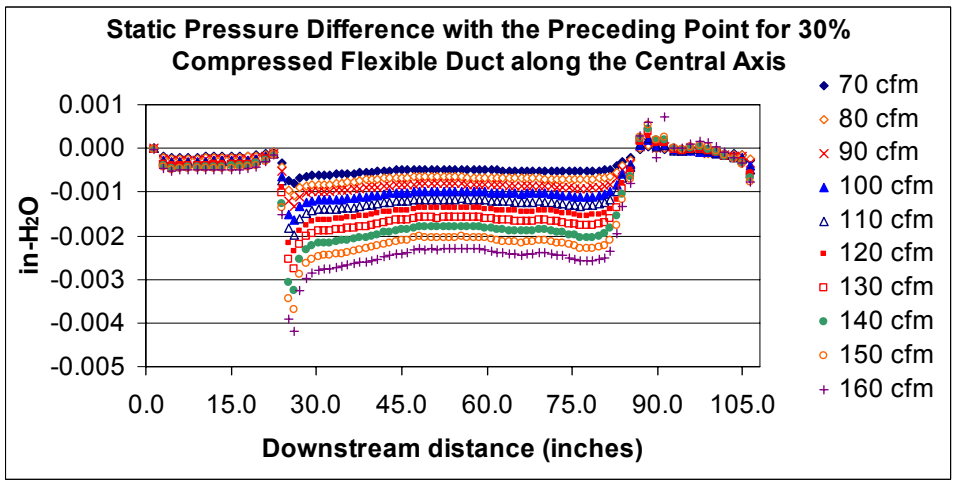

Figure 6d. Static pressure difference with the preceding data point of the 30% compressed flexible duct.

Comparison between CFD Simulations and Laboratory Data

In this section, results from CFD simulations were compared to the laboratory experiments. Three types of data, which were gathered from simulations, were used for comparison. Static pressure drop across 5', 4', and 3' length flexible duct was derived. Figure 7 shows the position of the duct portion used for this purpose. ΔP for those three duct sections were multiplied by 20, 25 and 33.33, respectively, to fit in-H_20/100' standard. This procedure was repeated for all four duct configurations which were simulated under ten volumetric air-flows.

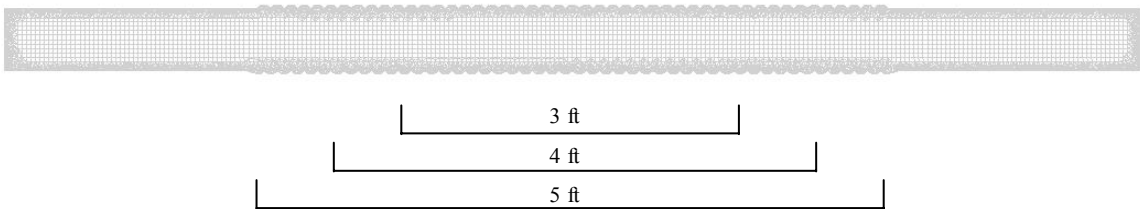

Figure 7. Three duct sections used for analysis.

The extrapolated simulation results were then compared to laboratory data. Table 2 shows the difference between ΔP from CFD simulations and ΔP from laboratory data (ΔP_{CFD} - ΔP_{Lab}). Ideally the difference should be very close to 0 for all conditions. In this study, simulation results of 30% configuration were as close as 0.0041 in-H_20 (0.78%) to laboratory data. In general, maximum stretched and 30% compressed configurations showed close agreement with the laboratory experiments. However, 4% and 15% compressed configurations showed higher deviations. The extrapolated data from the 3' length section resulted in closest agreement compared to the 4 and 5' length sections. Figure 8 shows a comparison between the simulation results and the laboratory data based on a 3' length duct. In the final section of this paper, a correction factor will be presented for 4% and 15% compressed configurations which will bring the data to close agreement.

TABLE 2
ΔP Difference between CFD Simulations and Laboratory Experiments Based on Three CFD Duct Lengths Projected to fit in-H2O/100' standard (ΔP_{CFD} - ΔP_{Lab})

cfm	70	80	90	100	110	120	130	140	150	160
MaxStretch based on 5 ft.	0.0351	0.0360	0.0418	0.0415	0.0449	0.0464	0.0455	0.0440	0.0376	0.0370
MaxStretch based on 4 ft.	0.0341	0.0335	0.0383	0.0395	0.0444	0.0429	0.0435	0.0410	0.0336	0.0325
MaxStretch based on 3 ft.	0.0324	0.0327	0.0391	0.0395	0.0402	0.0404	0.0402	0.0393	0.0336	0.0283
4% based on 5 ft.	0.1566	0.1964	0.2425	0.2881	0.3404	0.3941	0.4509	0.5230	0.5874	0.6465
4% based on 4 ft.	0.1496	0.1854	0.2295	0.2726	0.3204	0.3711	0.4249	0.4895	0.5524	0.6045
4% based on 3 ft.	0.1412	0.1770	0.2211	0.2634	0.3070	0.3560	0.4082	0.4702	0.5306	0.5810
15% based on 5 ft.	0.3193	0.4050	0.4722	0.5675	0.6624	0.7529	0.7976	0.8769	0.9752	1.0639
15% based on 4 ft.	0.3113	0.3945	0.4562	0.5460	0.6359	0.7184	0.7516	0.8229	0.9107	0.9894
15% based on 3 ft.	0.2879	0.3636	0.4195	0.5001	0.5816	0.6541	0.6748	0.7394	0.8163	0.8850
30% based on 5 ft.	0.1337	0.1620	0.1522	0.1709	0.1177	0.1024	0.1107	0.0849	-0.0076	-0.1397
30% based on 4 ft.	0.1147	0.1375	0.1217	0.1314	0.0702	0.0419	0.0397	-0.0041	-0.1091	-0.2547
30% based on 3 ft.	0.1030	0.1199	0.1041	0.1121	0.0476	0.0176	0.0145	-0.0360	-0.1452	-0.2933

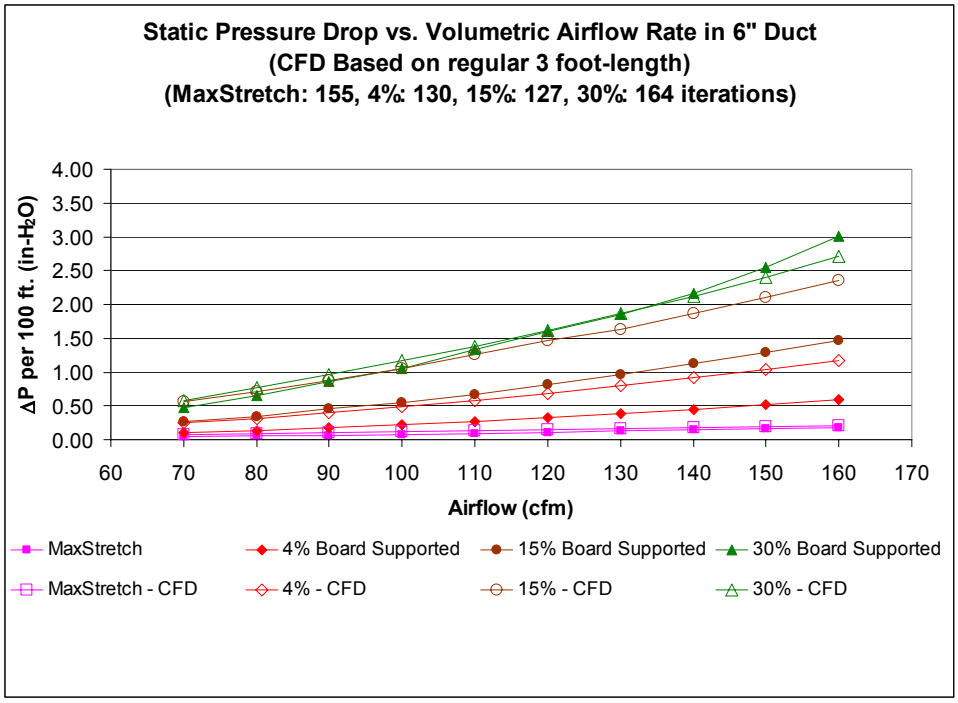

Figure 8. Comparison between simulation results and laboratory data based on a 3' length duct.

Comparison between Alternative 3' Long Duct and Laboratory Data

In Figures 6a through Figure 6d, the static pressure differences between two consecutive data points were plotted for all four duct configurations. These figures suggest that flow develops inside the duct approximately after one-fifth of the flexible duct section. Part of the 3', 4', and 5' length duct sections, which are symmetrical to the mid-point of the total duct length, fall into the less developed regions of the air-flow. The potential effects of this situation on the projected results were investigated. For this purpose, alternative 3' length duct sections were chosen which are situated under more developed regions of the airflow. These sections are between 49.50 – 85.50 in., 45.60 – 81.60 in., 41.85 – 77.55 in., and 40.80 – 76.50 in. for maximum stretched, 4%, 15%, and 30% compressed duct configurations, respectively. ΔP_{CFD} - ΔP_{Lab} for alternative and symmetrical duct sections are tabulated in Table 3. This test decreased ΔP of the CFD simulations by the order of approximately 0.01 in-H_2O. This difference affected maximum stretched and 4% compressed configurations more, due to their relatively smaller ΔP. However, this alternative duct length didn't make significant differences for 15% and 30% compressions. The results are presented graphically in Figure 9. The conclusion from this test is that whether the flow is fully developed or not has very little effect on our model.

TABLE 3
ΔP Difference between CFD Simulations and Laboratory Experiments Based on Regular and Alternative 3' Long Duct Projected to fit in-H2O/100' standard ($\Delta P_{CFD} - \Delta P_{Lab}$)

cfm	70	80	90	100	110	120	130	140	150	160
MaxStretch based on 3 ft.	0.0324	0.0327	0.0391	0.0395	0.0402	0.0404	0.0402	0.0393	0.0336	0.0283
MaxStretch based on 3 ft. (alternative)	0.0224	0.0227	0.0258	0.0228	0.0236	0.0204	0.0202	0.0160	0.0069	0.0050
4% based on 3 ft.	0.1412	0.1770	0.2211	0.2634	0.3070	0.3560	0.4082	0.4702	0.5306	0.5810
4% based on 3 ft. (alternative)	0.1279	0.1604	0.1945	0.2301	0.2670	0.3094	0.3482	0.4036	0.4540	0.4911
15% based on 3 ft.	0.2879	0.3636	0.4195	0.5001	0.5816	0.6541	0.6748	0.7394	0.8163	0.8850
15% based on 3 ft. (alternative)	0.2912	0.3669	0.4228	0.5034	0.5849	0.6574	0.6648	0.7260	0.7963	0.8583
30% based on 3 ft.	0.1030	0.1199	0.1041	0.1121	0.0476	0.0176	0.0145	-0.0360	-0.1452	-0.2933
30% based on 3 ft. (alternative)	0.0996	0.1199	0.1041	0.1088	0.0442	0.0109	0.0045	-0.0493	-0.1585	-0.3066

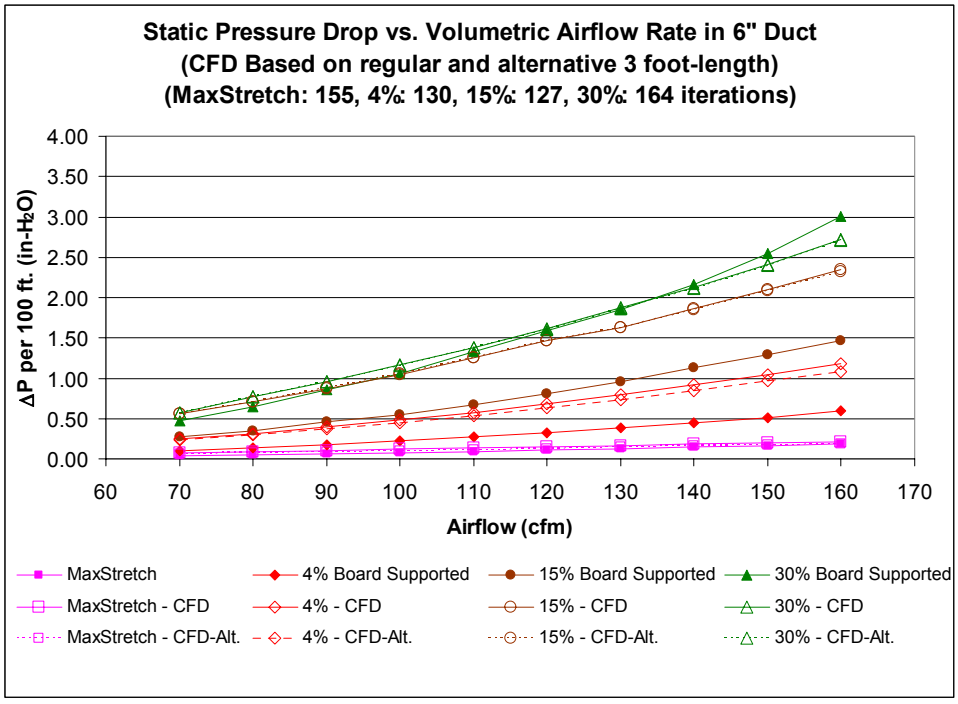

Figure 9. Comparison between regular and alternative 3' length duct and laboratory experiments.

Correction Factor for 4% and 15% Compressions

As stated earlier, under the same simulation conditions, 4% and 15% compressed duct simulations showed higher deviation from the laboratory results than fully-stretched and 30% compressions. We derived similar curves yet higher ΔPs from CFD for 4% and 15% compared to laboratory data. Multipliers were applied to CFD results of 4% and 15% to eliminate the discrepancy between the CFD and laboratory studies and are presented in Figure 10a and Figure 10b. According to this test, it is concluded that we can bring 4% and 15% CFD data to close agreement with laboratory data by applying 0.5 and 0.6 as multipliers, respectively.

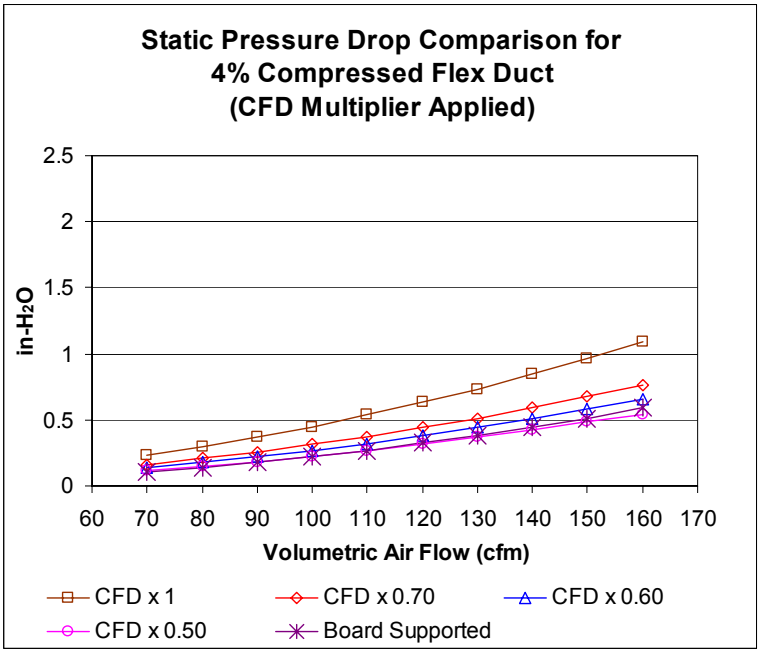

Figure 10a. Multiplier test for 4% compressed flexible duct.

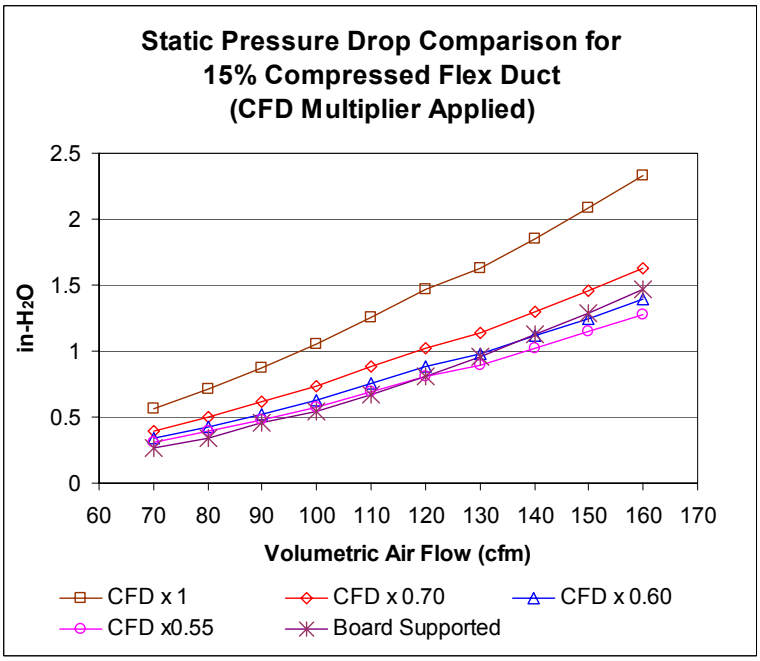

Figure 10b. Multiplier test for 15% compressed flexible duct.

CONCLUSION

Fully stretched, 4%, 15% and 30% compressed 6" flexible duct configurations were simulated using CFD software under various volumetric air-flows. CFD simulation results showed close proximity to laboratory experiments for fully-stretched and 30% configurations. However, considerably higher results were derived for 4% and 15% configurations. It is concluded from the comparisons that calculations based on the 3' length section have the most accuracy compared to the 4' and 5' length sections. An alternative 3' length duct section was selected on the same models to test the effect of developed air-flow on the final results. This test resulted in very minor improvements on the model. In the last section, correction factors were applied to 4% and 15% simulation results which brought them in close agreement to laboratory data. In these CFD simulations, we applied the standard k-e turbulence model. Further research is needed to determine why the 4% and 15% CFD data do not agree with the experimental data. Also, further studies on the turbulence model are noted as future research of this study. Finally, it is concluded that CFD models, developed in this study based on a 3' length section, can be used for design purposes of board supported configuration of fully stretched, 4%, 15% and 30% compressed flexible ducts. At this point, a comparative study between CFD simulations and laboratory experiments of joist supported flexible duct configuration, which has sag, is also noted as future work.

REFERENCES

Abushakra, B., I. S. Walker, M. H. Sherman. 2004. Compression Effects on Pressure Loss in Flexible HVAC Ducts. International Journal of Heating, Ventilating, Air-Conditioning and Refrigeration Research, 10(3): 275 – 289.

ASHRAE. 2005. ASHRAE Handbook of Fundamentals. American Society of Heating Refrigerating and Air-conditioning Engineers, Atlanta, Georgia.

Drori, U., V. Dubovsky and G. Zisking. 2005. Experimental Verification of Induced Ventilation. Journal of Environmental Engineering, May 2005: 820-826.

Fluent. 2004. Release 6.2.16, Fluent Inc., USA.

Fluent. 2005. Fluent 6.2 User's Guide, Fluent Inc., USA.

Gambit. 2004a. Release 2.2.30, Fluent Inc., USA.

Gambit. 2004b. Gambit 2.2.30 User's Guide, Fluent Inc., USA.

Gan, G. and S. B. Riffat. 1995. k-factors for HVAC ducts: Numerical and Experimental Determination. Building Services Engineering Research & Technology, 16(3):133-139.

Koskela, H. 2004. Momentum Source Model for CFD-simulation of Nozzle Duct Air Diffuser. Energy and Buildings, 36: 1011-1020.

Ugursal, A. and C. Culp. 2006. Comparative Study: CFD ΔP versus Measured ΔP for 30% Flexible Ducts. Proceedings of the Fifteenth Symposium on Improving Building Systems in Hot and Humid Climates. Orlando, FL

Weaver, K. and C. Culp, Private communication on study results which are submitted for publication.

Zhang, L. 2005. Turbulent Three-dimensional Air Flow and Heat Transfer in a Cross-corrugated triangular duct . Journal of Heat Transfer, 127:1151-1158.